Networks and Heterogeneous Media
Vol. 17, No. 3, June 2022, pp. 333–357
doi:10.3934/nhm.2022010

MATHEMATICAL ANALYSIS OF A HYBRID MODEL: IMPACTS OF INDIVIDUAL BEHAVIORS ON THE SPREADING OF AN EPIDEMIC

Guillaume Cantin

Laboratoire des Sciences du Numérique, LS2N UMR CNRS 6004
Université de Nantes, France

Cristiana J. Silva*

Center for Research and Development in Mathematics and Applications (CIDMA)
Department of Mathematics, University of Aveiro
3810-193 Aveiro, Portugal

and Arnaud Banos

UMR IDEES, CNRS, 25 rue Philippe Lebon BP 1123
76063 Le Havre Cedex, UK

Abstract. In this paper, we investigate the well-posedness and dynamics of a class of hybrid models, obtained by coupling a system of ordinary differential equations and an agent-based model. These hybrid models intend to integrate the microscopic dynamics of individual behaviors into the macroscopic evolution of various population dynamics models, and can be applied to a great number of complex problems arising in economics, sociology, geography and epidemiology. Here, in particular, we apply our general framework to the current COVID-19 pandemic. We establish, at a theoretical level, sufficient conditions which lead to particular solutions exhibiting irregular oscillations and interpret those particular solutions as pandemic waves. We perform numerical simulations of a set of relevant scenarios which show how the microscopic processes impact the macroscopic dynamics.

1. **Introduction.** The intricate and fascinating relations between the individual and collective behaviors, occurring within a population subject to an evolution problem, have been widely studied for several decades in the field of sociology and economics. Beyond the inescapable textbook of Turner & Killian [37], which is devoted to the study of social collective behaviors, these intricate relations within gatherings, demonstrations and riots have been analyzed, for example in [29] or [38]; self-organization of complex structures, admitting individual or collective social organization, have been studied in [33]; competition between individual and collective behaviors acting in segregation processes have been explored in [18]; more recently, individual roles in collective dynamics or in consensus emergence have been investigated in [26] or in [12]; finally, Galam [17] and Helbing [20] propose to regroup these various questions in a more general framework. However, it is observed that

2020 *Mathematics Subject Classification.* Primary: 34F05, 34A38; Secondary: 91C99.
Key words and phrases. Hybrid model, networks, agent-based model, multi-scale, epidemics.
* Corresponding author: Cristiana J. Silva.

the classical mathematical modelling approaches (especially those using ordinary differential equations) show limitations for reproducing the complex interactions between individual behaviors and collective dynamics. A very simple reason can account for this lack: although ordinary differential equations provide a powerful tool for describing the evolution of population dynamics, it is impossible to follow the trajectory of a single individual within the aggregate flow of such equations. Next, the observation of such real-world phenomena reveals the interleaving of at least two populational scales: the macroscopic scale can be used to describe collective behaviors, whereas the microscopic scale can fit with individuals decisions. Hence, coupling both the macroscopic and microscopic approaches is an attempt to overcome the scaling dilemma. Furthermore, none of both microscopic and macroscopic modelling approaches is better than the other; each one has advantages and disadvantages. However, the differential equations approach offers a formal study potential, which allows to establish qualitative properties of the trajectories determined by the resulting model, at a theoretical level. Thus it appears as a necessity, for the one who aims to advance on this modelling question, to couple ordinary differential equations with a microscopic process. It is precisely the purpose of this work.

Therefore, in this paper, we study a class of hybrid problems, constructed to model the complex features of population dynamic problems, in which the microscopic individual behaviors and the macroscopic collective dynamics are closely intertwined. We consider a general hybrid model, obtained by coupling a system of ordinary differential equations and an agent-based process, which act simultaneously along a common timeline. The complex network structure heavily underlies our hybrid model. Indeed, the subsequent system of ordinary differential equations is embedded into a geographical network structure, so as to reproduce the spatial background of the population dynamics, which possibly present heterogeneous patterns and emergent properties; in parallel, the social interactions occurring between individuals are supported by a social network, which can be partly randomly generated. The resulting mathematical model is analyzed both at a theoretical level and with a numerical approach. The way our model is designed allows its application to a large number of evolution problems arising, for example, in sociology, economics, geography and epidemiology. In this paper, we apply our general model to the current COVID-19 pandemic, whose complex dynamics have been intensely studied.

Besides the general framework of the proposed hybrid models, our approach aims to fill important limitations of previous studies on the topic of epidemics. Indeed, the macroscopic dynamics of epidemics have been intensely studied, using differential equations, very often on the basis of the famous Kermack & McKendrick model [25] (see, for instance, [22], [23], [35] or [36]). Partial differential equations, such as reaction-diffusion equations, have also been used in order to analyze the spatial propagation of epidemics as travelling waves (see for instance [13], [24] or [30]). Recently, epidemiological problems have benefited from the advances on the study of complex networks, which have been used in order to analyze the geographical spreading of various infectious diseases with a different approach (see for instance [7], [9], [27] or [34]). In the mean time, but separately, agent-based models have been used in order to study the microscopic dynamics of epidemics at the individual scale (see for instance [5] or [21]); in particular, agent-based stochastic-process

compartmental models have been studied in [2], [3] or very recently in [39]. Afterwards, a first attempt to compare both macroscopic and microscopic approaches is presented in [14], with the aim to establish the importance to take into account the role of individual behaviors. The necessity of coupling differential equations with agent-based models is finally highlighted in ecology (see e.g., [16], [28], [32]) and in epidemiology (see e.g., [1], [4]). However, these studies often lack for a theoretical mathematical validation; for example, the hybrid mathematical model which is studied in the latter paper [4] has not been validated in a theoretical framework and the qualitative properties of its solutions have not been analyzed. Hence, in this article, we do an in-depth study of such hybrid models and fill these temporary deficiencies.

In this paper, we pursue two main objectives. First, we intend to propose a sufficiently large framework which can be applied to a great number of complex problems arising in social and human sciences, and not only in epidemiology, with a rigorous mathematical approach, which supports the numerical simulations and guarantees their relevancy. For that, we construct an abstract class of hybrid models by coupling along a common timeline a macroscopic and continuous process, determined by a system of differential equations, with a microscopic and discrete process, which can be derived from an agent-based model. Under reasonable assumptions, we prove that the resulting hybrid model is well-posed, in the sense that it admits global solutions (see Theorem 2.2), which depend smoothly on a variation of its parameters (see Theorem 2.3). We also prove that the system can exhibit particular solutions with irregular oscillations, (see Theorem 2.4), that generalizes a previous statement presented in [34]. Secondly, we apply our general framework to the current COVID-19 pandemic, so as to prove that the dynamics, spreading and multiple waves of this devastating pandemic cannot be explained only at a macroscopic scale. We use a deterministic ODE compartmental model earlier presented in [35], which is designed for reproducing the specificity of transmission of SARS-CoV-2 virus in a susceptible population, and an agent-based process which focuses on refractory behaviors of citizens to policy strategies. We present several numerical simulations of the hybrid model which highlight the effect of such opposition behaviors on the aggregate flow of the epidemic.

Our paper is organized as follows. In Section 2, we show how to construct the general hybrid model, by coupling a system of differential equations and an agent-based model; we prove that the resulting mathematical problem is well-posed. Next, in Section 3, we apply our general framework to the current COVID-19 pandemic, for which the macroscopic dynamic is described by a deterministic ODE compartmental model, whereas the microscopic opposition behaviors and decision strategies are integrated into an agent-based protocol. The stability analysis of the model is investigated in 4, and a selection of relevant scenarios are finally presented in Section 5 with a numerical approach.

2. **Hybrid models in a general context.**

In this section, we provide a theoretical mathematical approach to a class of abstract hybrid problems. To construct the hybrid problems, we couple a system of ordinary differential equations with a discrete process, along a common timeline. After, we prove the well-posedness of the resulting mathematical problem and, under reasonable assumptions, the existence of irregular oscillations.

2.1. **Construction of a class of abstract hybrid models.** Let us consider a population of individuals and assume that this population is subject to a complex evolution process which cannot be described at a single scale. Thus, we construct a hybrid model by coupling a system of ordinary differential equations and a discrete process, which can be derived from an agent-based model.

First, we assume that the population can be divided into several disjoint groups $x_1, \ldots, x_n$ $(n \geq 1)$ and introduce the notation $X = (x_1, \ldots, x_n)^\top$. Next, we consider a discrete sequence of times

$$t_0 < t_1 < \cdots < t_s < t_{s+1} < \ldots, \tag{1}$$

which tends to infinity. We consider the following abstract hybrid problem (AHP)

$$\begin{cases} (\mathfrak{IC}) & X(t_0) = X_0, \quad \lambda_0 \in J, \\ (\mathfrak{M}_s) & \dot{X}(t) = F\big(X(t), \lambda_s\big), \quad t_s < t \leq t_{s+1}, \\ (\mathfrak{m}_s) & \lambda_{s+1} = G\big(X(t_{s+1}), \lambda_s\big), \end{cases} \tag{AHP}$$

for $s \geq 0$. Here, F is a function defined in $E \times J$ with values in $\mathbb{R}^n$, where E is an open subset of $\mathbb{R}^n$ and J is an open subset of $\mathbb{R}^d$; G is a function defined in $E \times J$ with values in J. The first line $(\mathfrak{IC})$ in system (AHP) determines the initial condition $(X_0, \lambda_0) \in E \times J$; the second line $(\mathfrak{M}_s)$ is an ordinary differential equation which determines the macroscopic part of the hybrid problem, whereas the third line $(\mathfrak{m}_s)$ is a discrete mapping which determines the microscopic part of the hybrid problem.

The hybrid problem (AHP) can be applied to a great number of population dynamics problems arising in sociology, economics, geography or epidemiology. In particular, we shall study in the next section an application of the hybrid model (AHP) to the current COVID-19 pandemic; the macroscopic part $(\mathfrak{M}_s)$ will be given by a deterministic ODE compartmental model for the transmission of SARS-CoV-2, whereas the microscopic part $(\mathfrak{m}_s)$ will follows from an explicit agent-based model.

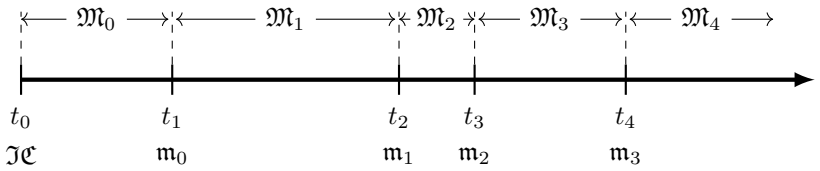

FIGURE 1. Timeline of the hybrid model (AHP). At $t = t_0$, the initial condition $(\mathfrak{IC})$ gives $(X_0, \lambda_0) \in E \times J$. On each interval $[t_s, t_{s+1}]$, the macroscopic part $(\mathfrak{M}_s)$ is determined by an ordinary differential equation. At each time step $t = t_s$, the microscopic part $(\mathfrak{m}_s)$ follows from a discrete mapping which is derived from an agent-based model.

Definition 2.1. For $(X_0, \lambda_0) \in E \times J$, a global solution of the hybrid problem (AHP) is a pair denoted $\big(X(t, X_0), (\lambda_s)_{s\geq 0}\big)$ in which $X(t, X_0)$ is a function of t defined and differentiable in $[t_0, +\infty)$, such that $X(t_0, X_0) = X_0$ and satisfying $(\mathfrak{M}_s)$ on $(t_s, t_{s+1}]$ for all $s \geq 0$; $(\lambda_s)_{s\geq 0}$ is a sequence of parameters in J satisfying $(\mathfrak{m}_s)$ for all $s \geq 0$.

For brevity, a solution of the hybrid problem (AHP) starting from (X_0, λ_0) shall be denoted as $X(t, X_0, \lambda_0)$.

2.2. **Well-posedness of the hybrid model** (AHP)**.** In order to establish the well-posedness of the hybrid model (AHP), we consider the three following assumptions.

Assumption 1. The function F involved in the macroscopic part $(\mathfrak{M}_s)$ of the hybrid problem (AHP) is $\mathscr{C}^1(E \times J)$.

Assumption 2. There exists a compact set $K \subset E$ such that, for all $(X_0, \lambda_0) \in K \times J$, each local solution $X(t, X_0)$ of the Cauchy problem

$$X(t_0) = X_0, \quad \dot{X}(t) = F\big(X(t), \lambda_0\big)$$

defined on $[t_0, t_0 + T]$ with $T > 0$ satisfies

$$X(t, X_0) \in K,$$

for all $t \in [t_0, t_0 + T]$.

Note that in assumption 2, the compact set K does not depend on the initial condition (X_0, λ_0).

Assumption 3. The function G involved in the microscopic part $(\mathfrak{m}_s)$ of the hybrid problem (AHP) is continuous in $E \times J$.

Our first theorem establishes the existence and uniqueness of global solutions to the hybrid problem (AHP).

Theorem 2.2. *Let the assumptions 1 and 2 hold. Then for all $(X_0, \lambda_0) \in K \times J$, the hybrid problem* (AHP) *admits a unique global solution $X(t, X_0, \lambda_0)$ defined on $[t_0, +\infty)$, in the sense of Definition 2.1.*

Proof. In order to prove the theorem, we construct a solution to the hybrid problem (AHP) successively on each time interval $[t_s, t_{s+1}]$, with $s \geq 0$.

Let $(X_0, \lambda_0) \in E \times J$. We first consider the Cauchy problem on the time interval $[t_0, +\infty)$:

$$X(t_0) = X_0, \quad \dot{X}(t) = F\big(X(t), \lambda_0\big), \quad t > 0. \tag{2}$$

By virtue of Assumption 1, it follows from the fundamental existence and uniqueness theorem for ordinary differential equations (see for instance Theorem 3.1 in [19]), that the Cauchy problem (2) admits a unique local solution $\tilde{X}(t, X_0)$ defined on $[t_0, t_0 + T]$ with $T > 0$. Furthermore, Assumption 2 guarantees that this solution is global, that is $T = +\infty$. Thus, we define a unique solution of the hybrid problem (AHP) on $(t_0, t_1]$ by setting $X(t, X_0, \lambda_0) = \tilde{X}(t, X_0)$, $t_0 < t \leq t_1$, $X_1 = X(t_1, X_0, \lambda_0)$ and $\lambda_1 = G\big(X_1, \lambda_0\big)$.

Afterwards, assuming that $X(t, X_0, \lambda_0)$ has been defined on $[t_0, t_s]$ with $s \geq 1$, we set $X_s = X(t_s, X_0, \lambda_0)$, $\lambda_s = G\big(X_s, \lambda_{s-1}\big)$ and consider the Cauchy problem on the time interval $[t_s, +\infty)$:

$$X(t_s) = X_s, \quad \dot{X}(t) = F\big(X(t), \lambda_s\big), \quad t > t_s.$$

Repeating the above arguments, we construct a unique solution of the hybrid problem (AHP) on $[t_0, t_{s+1}]$, for all $s \geq 1$. In this way, we have constructed a unique global solution of the hybrid problem (AHP) in the sense of Definition 2.1. □

The next theorem establishes the continuity of the solution $X(t, X_0, \lambda_0)$ of the hybrid problem (AHP) with respect to a variation of the initial condition $X_0 \in K$ and of the initial parameter value $\lambda_0 \in J$. This continuity principle validates in a rigorous mathematical framework the construction of the hybrid problem, which in turn allows multiple applications to real-world problems.

Theorem 2.3. *Let Assumptions 1, 2 and 3 hold. Then each global solution $X(t, X_0, \lambda_0)$ of the hybrid problem (AHP) is continuous at (X_0, λ_0), uniformly on each finite time interval $[t_0, t_0 + T]$ with $T > 0$, that is, for each $T > 0$ and each $\varepsilon > 0$, there exists $\delta > 0$ such that*

$$\|X(t, X_0 + h, \lambda_0 + k) - X(t, X_0, \lambda_0)\|_{\mathbb{R}^n} < \varepsilon,$$

for all $t \in [t_0, t_0 + T]$, provided that $\|(h, k)\|_{\mathbb{R}^n \times \mathbb{R}^d} < \delta$.

Proof. Let us consider $T > 0$, $(X_0, \lambda_0) \in K \times J$ and $\varepsilon > 0$. For each $(h, k) \in \mathbb{R}^n \times \mathbb{R}^d$ such that $(X_0 + h, \lambda_0 + k) \in K \times J$, we denote $\tilde{X}_0 = X_0 + h$, $\tilde{\lambda}_0 = \lambda_0 + k$, and $X(t, X_0, \lambda_0)$, $X(t, \tilde{X}_0, \tilde{\lambda}_0)$ the solutions of the hybrid problem (AHP) stemming from (X_0, λ_0) and $(X_0 + h, \lambda_0 + k)$ respectively. By virtue of Theorem 3.4 in [19], there exists $\delta > 0$ such that

$$\left\| X(t, \tilde{X}_0, \tilde{\lambda}_0) - X(t, X_0, \lambda_0) \right\|_{\mathbb{R}^n} < \varepsilon,$$

for all $t \in [t_0, t_1]$, provided that $\|(h, k)\|_{\mathbb{R}^n \times \mathbb{R}^d} < \delta$. It follows that

$$\left\| \tilde{X}_1 - X_1 \right\|_{\mathbb{R}^n} < \varepsilon,$$

where $\tilde{X}_1 = X(t_1, \tilde{X}_0, \tilde{\lambda}_0)$ and $X_1 = X(t_1, X_0, \lambda_0)$, for all $\varepsilon > 0$.

Next we consider $\lambda_1 = G(X_1, \lambda_0)$ and $\tilde{\lambda}_1 = G(\tilde{X}_1, \tilde{\lambda}_0)$. Diminishing ε and δ if necessary, by virtue of Assumption 3, we have that $\left\| \lambda_1 - \tilde{\lambda}_1 \right\|_{\mathbb{R}^d} < \xi$, for all $\xi > 0$.

Repeating these arguments a finite number of times, we have that for all $s \geq 1$ such that $t_s \in [0, T]$ and for all $\varepsilon > 0$, there exists $\delta > 0$ such that

$$\left\| X(t, \tilde{X}_0, \tilde{\lambda}_0) - X(t, X_0, \lambda_0) \right\|_{\mathbb{R}^n} < \varepsilon,$$

for all $t \in [t_0, t_s]$, provided that $\|(h, k)\|_{\mathbb{R}^n \times \mathbb{R}^d} < \delta$. □

Remark 1. If G is discontinuous, then the solution $X(t, X_0, \lambda_0)$ of the hybrid problem (AHP) can obviously be very sensitive to a perturbation of the initial parameter value λ_0. Indeed, let us assume that the differential equation $\dot{X} = F(X, \lambda)$ admits two equilibrium points Σ_1 and Σ_2, for two parameter values λ_1 and λ_2, respectively. Furthermore, let us assume that λ^* is a bifurcation value which separates λ_1 and λ_2. If two solutions $X(t, X_0, \lambda_0)$ and $\tilde{X}(t, \tilde{X}_0, \lambda_0)$ of the hybrid problem (AHP), stemming from two initial conditions X_0 and $\tilde{X}_0$, satisfy $\lambda_s < \lambda^* < \tilde{\lambda}_s$ for some $s > 0$, then $X(t, X_0, \lambda_0)$ and $\tilde{X}(t, \tilde{X}_0, \lambda_0)$ will be attracted towards Σ_1 and Σ_2, respectively, diverging from each other. Roughly speaking, if the microscopic part $(\mathfrak{m}_s)$ of the hybrid problem (AHP) is determined by a discontinuous mapping G, then its flow can be ripped into several sub-flows which diverge from each other.

2.3. **Existence of particular solutions of (AHP) exhibiting irregular oscillations.** In this section, we establish and interpret an important feature of the hybrid model (AHP), by proving the existence of particular solutions exhibiting irregular oscillations, under reasonable assumptions which we intend to present now.

Let us suppose that there exist two distinct parameters sets $\Lambda_1 \subset J$ and $\Lambda_2 \subset J$. Those parameters sets possibly satisfy $\Lambda_1 \cap \Lambda_2 = \varnothing$. Assume, moreover, that Σ_1 is an equilibrium point of the equation

$$\dot{X} = F(X, \lambda_1),$$

for each $\lambda_1 \in \Lambda_1$, and that Σ_2 is an equilibrium point of the equation

$$\dot{X} = F(X, \lambda_2),$$

for each $\lambda_2 \in \Lambda_2$. We introduce the minimum step of the timeline $\{t_s\}$ given by (1) by setting:

$$\tau = \min_{s \geq 0} |t_s - t_{s+1}|.$$

The next theorem generalizes a recent result proved in [34].

Theorem 2.4. *Suppose that assumption 2 holds. Assume that Σ_1 is globally asymptotically stable in $W_1 \subset K$ for each $\lambda_1 \in \Lambda_1$, Σ_2 is globally asymptotically stable in $W_2 \subset K$ for each $\lambda_2 \in \Lambda_2$. Assume moreover that $\Sigma_1 \in W_2$, $\Sigma_2 \in W_1$ and $G(Y, \lambda) \in \Lambda_2$ if Y is near Σ_1 and $\lambda \in \Lambda_1$, $G(Y, \lambda) \in \Lambda_1$ if Y is near Σ_2 and $\lambda \in \Lambda_2$.*

Then every solution $X(t, X_0, \lambda_0)$ of the hybrid problem starting from $(X_0, \lambda_0) \in W_1 \times \Lambda_1$ admits irregular oscillations, that is, oscillations between a neighborhood $\mathcal{N}_1$ of Σ_1 and a neighborhood $\mathcal{N}_2$ of Σ_2, provided the minimum step τ of the timeline is sufficiently large.

Proof. Let us consider $(X_0, \lambda_0) \in W_1 \times \Lambda_1$. Since Σ_1 is globally asymptotically stable in W_1, the solution of the Cauchy problem

$$X(t_0) = X_0, \quad \dot{X}(t) = F\big(X(t), \lambda_0\big), \quad t > 0,$$

belongs to a neighborhood $\mathcal{N}_1$ of Σ_1 after a finite time $T > 0$. Moreover, the minimum step τ of the timeline can be chosen arbitrarily large, thus we can assume that $\tau > T$. In this way, the solution $X(t, X_0, \lambda_0)$ of the hybrid problem (AHP) belongs to $\mathcal{N}_1$ for $t \in [\tau, \tau + \theta]$ with $\theta > 0$ such that $t_1 \in [\tau, \tau + \theta]$. Hence, the solution $X(t, X_0, \lambda_0)$ of the hybrid problem (AHP) satisfies $X_1 = X(t_1, X_0, \lambda_0) \in \mathcal{N}_1$.

Next, it is assumed that Σ_1 belongs to the basin of attraction W_2 of Σ_2; moreover, since $\lambda_0 \in \Lambda_1$, we have $G(Y, \lambda_0) \in \Lambda_2$ if Y is near Σ_1, thus $\lambda_1 = G(X_1, \lambda_0) \in \Lambda_2$. Since Σ_2 is globally asymptotically stable in W_2, we can repeat the above arguments to conclude that the solution of the hybrid problem $X(t, X_0, \lambda_0)$ reaches a neighborhood $\mathcal{N}_2$ of Σ_2 after a finite time $t_1 + T$ with $T > 0$, thus satisfies $X(t_2, X_0, \lambda_0) \in \mathcal{N}_2$. Since $\Sigma_2 \in W_1$, it follows that after a finite time $t_2 \in [t_1, t_1 + T]$, the solution $X(t, X_0, \lambda_0)$ of the hybrid problem (AHP) is back in the basin of attraction of Σ_1.

Since $G(Y, \lambda_2) \in \Lambda_1$ if Y is near Σ_1, we are brought back to an initial condition $(X_2, \lambda_2) \in W_1 \times \Lambda_1$ with $X_2 = X(t_2, X_0, \lambda_0)$ and $\lambda_2 = G(X_1, \lambda_1)$. Therefore, the solution $X(t, X_0, \lambda_0)$ of the hybrid problem (AHP) oscillates between $\mathcal{N}_1$ and $\mathcal{N}_2$, which completes the proof. □

Remark 2. Obviously, the conclusion of Theorem 2.4 still holds if the initial condition (X_0, λ_0) belongs to $W_2 \times \Lambda_2$. Furthermore, if the equation $\dot{X} = F(X, \lambda)$

admits more than two equilibrium points, then the solution $X(t, X_0, \lambda_0)$ of the hybrid problem (AHP) can exhibit more complex dynamics, with chaotic oscillations between more than two neighborhoods of equilibrium points.

Remark 3. In the sequel, our main application of the hybrid problem (AHP) is devoted to epidemic models; these epidemic models often admit a disease-free equilibrium and an endemic equilibrium, thus two equilibrium points Σ_1 and Σ_2, for two distinct parameter sets which are determined by the value of a basic reproduction number R_0. In this context, the existence of pseudo-periodic solutions can be interpreted as the risk of multiple epidemic waves. Assuming that the microscopic part $(\mathfrak{m}_s)$ is partly determined by the decisions of policy makers, the condition "$G(Y, \lambda) \in \Lambda_2$ if $\lambda \in \Lambda_1$ and Y is near Σ_1" means that the decisions switch the dynamics of the epidemic from one equilibrium to the other. Finally, the condition "τ is sufficiently large" can be interpreted as a slowness in the decision processes.

3. Hybrid model applied to COVID-19.

In this section, we present an important application of the hybrid framework, constructing an instance of the hybrid problem (AHP), designed for studying the evolution of COVID-19, whose dynamics cannot be described at a single scale. The macroscopic part $(\mathfrak{M}_s)$ is determined by a deterministic compartmental $SAIRP$ model for the transmission of SARS-CoV-2 with opposition behaviors, whereas the microscopic part $(\mathfrak{m}_s)$ follows from an agent-based model. Both microscopic and macroscopic parts of the problem are supported by a complex network structure.

3.1. $SAIRP$ model with opposition behaviors.

Let us consider a population of individuals affected by the COVID-19 pandemic, caused by the infection of SARS-CoV-2. In order to integrate the impact of refractory behaviors on the dynamics of the epidemic, we propose to improve the deterministic compartmental $SAIRP$ mathematical model, recently analyzed in [34]. This epidemiological model takes into account the transmission of SARS-CoV-2 virus in a population of susceptible individuals.

The followings assumptions are in agreement with the ones from [35]. The population is subdivided into five distinct classes: susceptible individuals (S); asymptomatic infected individuals (A); active infected individuals (I); removed (including recovered and COVID-19 induced deaths) (R); protected individuals (P). The total population, $N(t) = S(t) + A(t) + I(t) + R(t) + P(t)$, with $t \in [0, T]$ representing the time (in days) and $T > 0$, has a variable size where the recruitment rate Λ, and the natural death rate $\mu > 0$, are assumed to be constant. The susceptible individuals S become infected by contact with active infected I and asymptomatic infected individuals A, at a rate of infection $\beta \frac{(\theta A + I)}{N}$, where θ represents a modification parameter for the infectiousness of the asymptomatic infected individuals A. Only a fraction q of asymptomatic infected individuals A develop symptoms and are detected, at a rate v. Active infected individuals I are transferred to the recovered/removed individuals R, at a rate δ, by recovery from the disease or by COVID-19 induced death. A fraction p, with $0 < p < 1$, is protected from infection, by the application of non-pharmaceutical interventions, such as, physical distancing, limited size of indoor and outdoor gatherings, teleworking, regular cleaning of frequently-touched surfaces and appropriate ventilation of indoor spaces, mask use and hand washing (see e.g. [8, 15]), that prevent from being exposed to the

infection, and is transferred to the class of protected individuals P, at a rate ϕ. A fraction f of protected individuals P returns to the susceptible class S, at a rate w.

In addition to what was proposed in [34], we consider a fraction $u \in [0,1]$ of individuals who adopt refractory or opposition behaviors to the protection strategy. In this way, the transfer term from the susceptible class S to the protected class P is given by $\pm\phi p(1-u)S(t)$, and the infection term is modified in correspondence. In what follows, for the sake of simplification, we use the notation $\nu = vq$ and $\omega = wf$.

Overall, the $SAIRP$ model with refractory behaviors is determined by the following system of ordinary differential equations:

$$\begin{cases} \dot{S}(t) = \Lambda - \beta\big(1-p(1-u)\big)\frac{(\theta A(t)+I(t))}{N(t)}S(t) - \phi p(1-u)S(t) + \omega P(t) - \mu S(t), \\ \dot{A}(t) = \beta\big(1-p(1-u)\big)\frac{(\theta A(t)+I(t))}{N(t)}S(t) - \nu A(t) - \mu A(t), \\ \dot{I}(t) = \nu A(t) - \delta I(t) - \mu I(t), \\ \dot{R}(t) = \delta I(t) - \mu R(t), \\ \dot{P}(t) = \phi p(1-u)S(t) - \omega P(t) - \mu P(t). \end{cases} \tag{3}$$

The latter deterministic compartmental model can be written

$$\dot{x} = f(x,\alpha),$$

with $x = (S, A, I, R, P)^\top \in \mathbb{R}^5$,

$$\alpha = (\beta, p, \theta, \Lambda, \phi, \omega, \mu, \nu, \delta, u) \in \mathbb{R}^{10} \tag{4}$$

and $f(x,\alpha) = \big(f_j(x,\alpha)\big)^\top_{1\le j\le 5}$ with

$$\big(f_j(x,\alpha)\big)^\top_{1\le j\le 5} = \begin{bmatrix} \Lambda - \beta\big(1-p(1-u)\big)\frac{(\theta A+I)}{N}S - \phi p(1-u)S + \omega P - \mu S \\ \beta\big(1-p(1-u)\big)\frac{(\theta A+I)}{N}S - \nu A - \mu A \\ \nu A - \delta I - \mu I \\ \delta I - \mu R \\ \phi p(1-u)S - \omega P - \mu P \end{bmatrix}. \tag{5}$$

The equilibrium points and their stability analysis are studied in Section 4.

3.2. **Geographical network modeling the spatial distribution of the population.** In order to take into account the geographical distribution of the population which is affected by the epidemic, we propose to embed the latter $SAIRP$ model into a complex network structure. Thus we assume that the individuals are spatially distributed into a finite number of regions $D_1, \ldots, D_m$ with $m \ge 1$; some of these regions are interconnected and individuals present a spatial mobility from one region to another (an example of such a geographical network is depicted in Figure 6 below). Thus we introduce a matrix

$$L = \big(L_{i,k}\big)_{1\le i,k\le m} \tag{6}$$

of geographical connectivity, by setting $L_{i,k} = 1$ if the region D_k is connected to the region D_i $(i \ne k)$; $L_{i,k} = 0$ else; $L_{i,i} = -\sum_{k\ne i} L_{k,i}$ for $i = k$. In this way, the matrix L is a matrix whose sum of coefficients of each column is null.

Next, we divide the population into a finite number of regional sub-populations

$$X = (x_i)_{1\leq i\leq m},$$

where $x_i = (x_{i,j})_{1\leq j\leq 5}^{\top} = (S_i, A_i, I_i, R_i, P_i)^{\top} \in \mathbb{R}^5$ denotes the population of the region D_i, $1 \leq i \leq m$.

In this way, the dynamics of the epidemic is modeled at the macroscopic scale by a complex network of ordinary differential equations, which is written

$$\frac{dx_{i,j}}{dt}(t) = f_j\big(x_i(t), \alpha_i\big) + \sigma_j \sum_{k=1}^{n} L_{i,k} x_{j,k}(t), \quad 1 \leq j \leq 5, \quad 1 \leq i \leq m, \quad t \geq 0. \tag{7}$$

Here, $f = (f_j)_{1\leq j\leq 5}$ is the function defined by (5) in $\mathbb{R}^5 \times \mathbb{R}^{10}$, with $1 \leq j \leq 5$, and $\alpha_i \in \mathbb{R}^{10}$ is the vector parameter given by (4). The vector-valued function $f = (f_j)_{1\leq j\leq 5}$ models the dynamic of the epidemic in each region. Since the dynamic is likely to differ from one region to another, the parameters α_i can be distinct for two different regions. The parameters σ_j are non-negative coefficients and model the rate of mobility of the regional sub-populations $x_{i,j}$ of type j, $1 \leq i \leq m$.

The problem (7) can be rewritten into the short form

$$\dot{X} = F(X, \lambda), \tag{8}$$

with $X = (x_i)_{1\leq i\leq m} \in \mathbb{R}^{5m}$, F is defined by

$$F(X, \lambda) = \left(f_j\big(x_i, \alpha_i\big) + \sigma_j \sum_{k=1}^{n} L_{i,k} x_{j,k} \right)_{1\leq j\leq m}^{\top}, \tag{9}$$

and

$$\lambda = \big((\alpha_i)_{1\leq i\leq m}, (\sigma_j)_{1\leq j\leq 5}, (L_{i,k})_{1\leq i,k\leq m}\big) \in \mathbb{R}^{10m+5+m^2},$$

thus, it is an instance of the macroscopic part $(\mathfrak{M}_s)$ of the hybrid problem (AHP) (see Section 2), with $n = 5m$ and $d = 10m + 5 + m^2$.

3.3. **Transition from a system of ordinary differential equations towards an agent-based model.** After having determined the macroscopic part $(\mathfrak{M}_s)$ of the hybrid model (AHP), our aim is now to construct the microscopic part $(\mathfrak{m}_s)$. However, two elementary obstacles should be overcome. Indeed, it is worth emphasizing that the differential equation approach is an aggregate approach in which it is impossible to follow the trajectory of a single individual. Furthermore, stemming from an integer number of individuals, the output of the differential equation leads to real numbers which are delicate to interpret. This modeling question has been studied in [4] by prioritizing an important constraint in their case (conservation of population) and therefore by adopting rough approximations, implying a loss of information.

Here, we consider an agent-based process in which agents are determined by *non-integer* individuals. Let us describe our approach. Assume we have solved system (8) on a finite time interval $[t_s, t_{s+1}]$, with $s \geq 0$, and denote by $X(t, X_s, \lambda_s)$ the corresponding orbit. For each sub-population x_{ij} of type j, $1 \leq j \leq 5$, in each region D_i, $1 \leq i \leq m$, we evaluate $x_{ij}(t_{s+1})$ and we compute the floor value $N_{ij}(t_{s+1}) = \lfloor x_{ij}(t_{s+1}) \rfloor$. We then consider a finite set

$$\mathfrak{A}_{ij} = \big\{\mathfrak{a}_{ij}^1, \mathfrak{a}_{ij}^2, \ldots, \mathfrak{a}_{ij}^{N_{ij}}\big\},$$

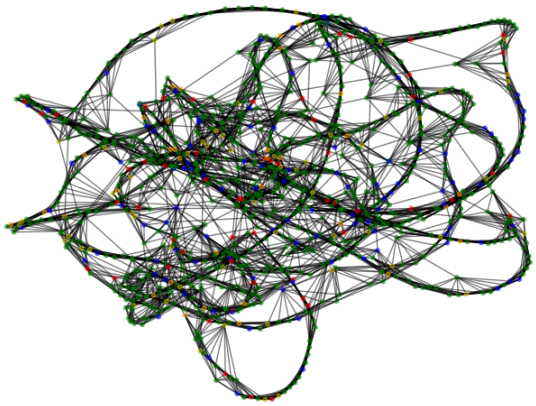

FIGURE 2. Social network generated over a finite set of agents, by running a Newman–Watts-Strogatz graph generation algorithm: each vertex represents an agent, and each edge models a social connection between two agents. Different colors correspond to the different epidemic sub-classes of the population. In such a social network, each agent can observe the types and the behaviors of its neighbors and can make decisions with respect to its observations.

and we call its elements *non-integer individuals* or simply *agents*. As constructed, the set $\mathfrak{A}_{ij}$ admits N_{ij} agents, which model the individuals of the sub-population x_{ij} $(1 \leq i \leq m,\, 1 \leq j \leq 5)$. In parallel, the size of the population at time $t = t_{s+1}$ is stored in the vector $X_{s+1} = X(t_{s+1}, X_s, \lambda_s)$, which is the initial condition for the next instance of the macroscopic part $(\mathfrak{M}_s)$ on the time interval $[t_{s+1}, t_{s+2}]$. The set $\mathfrak{A}_{ij}$ is called the *group of agents* $\mathfrak{a}_{ij}^g$ *in the sub-population of type* j *in region* D_i, $1 \leq g \leq N_{ij}$. We then generate a social network over the groups $(\mathfrak{A}_{ij})_{1\leq j\leq 5}$ of each region D_i, $1 \leq i \leq m$, by running a graph generation algorithm of edges over the finite set

$$\mathfrak{A}_i = \bigcup_{1\leq j\leq 5} \mathfrak{A}_{ij}. \tag{10}$$

Here, we choose to generate a Newman–Watts–Strogatz small-world graph, since it is well recognized to reproduce important aspects of the structure of social interactions [31]. However, other graph generation algorithms could be considered. In this social network, each agent has a finite number of neighbors; each agent can observe the types of its neighbors and make decisions, as illustrated in Figure 2. The microscopic part $(\mathfrak{m}_s)$ of the hybrid model (AHP) is finally determined by a decision protocol which we intend to describe in the following section.

3.4. **Agent-based model approach for integrating the collective behaviors in response to the epidemic.** Let us finally describe the agent-based model which is performed at each time step t_s of the time line (1). Assume that the system (8) has been solved on a time interval $[t_s, t_{s+1}]$ with the parameter values

$$\lambda_s = \Big\{ \big(\alpha_i(t_s)\big)_{1\leq i\leq m}, \big(\sigma_j(t_s)\big)_{1\leq j\leq 5}, \big(L_{i,k}(t_s)\big)_{1\leq i,k\leq m} \Big\},$$

and that the social network of agents $\mathfrak{A}_{ij}$ has been generated at time step t_{s+1}.

We assume that agents model citizens or decision makers and focus on two types of actions.

- *Action 1.* In each region D_i, $1 \leq i \leq m$, decision makers evaluate the rate $\rho_I(D_i, t_{s+1})$ of infected individuals; this rate is given by

$$\rho_I(D_i, t_{s+1}) = \frac{I_i(t_{s+1})}{N_i(t_{s+1})}. \tag{11}$$

  - If the rate $\rho_I(D_i, t_{s+1})$ overcomes a given threshold $\mathcal{T}_1$, that is $\rho_I(R_i, t_{s+1}) > \mathcal{T}_1$, then decision makers decide to increase the fraction p_i of individuals in region D_i which are protected. This increase is determined by the mapping

$$p_{i+1}(t_{s+1}) = p_i(t_s) \times (1 + d_1),$$

    where d_1 is a decision parameter such that $0 < d_1 < 1$.
  - Else, that is, if $\rho_I(D_i, t_{s+1}) \leq \mathcal{T}_1$, then the fraction of protected individuals is maintained, that is

$$p_{i+1}(t_{s+1}) = p_i(t_s).$$

  - If at least one of the rates $\rho_I(D_i, t_{s+1})$, $1 \leq i \leq m$, overcomes a second threshold $\mathcal{T}_2 > \mathcal{T}_1$, that is $\rho_I(D_i, t_{s+1}) > \mathcal{T}_2$ for at least one $i \in \{1, \ldots, m\}$, then decision makers decide to confine the individuals in their region, which is determined by setting

$$\sigma_j(t_{s+1}) = 0, \quad 1 \leq j \leq 5.$$

  - Else, that is, if $\rho_I(D_i, t_{s+1}) \leq \mathcal{T}_2$ for all $i \in \{1, \ldots, m\}$, then decision makers reestablish the last positive value of σ_j, $1 \leq j \leq 5$.
- *Action 2.* In each region D_i, $1 \leq i \leq m$, agents $\mathfrak{a}_{ij}^g$ of each type j, $1 \leq g \leq N_{ij}$, observe the types of their neighbors: S_i, A_i, I_i, R_i or P_i. Among these neighbors, each agent $\mathfrak{a}$ evaluates the number $\mathfrak{N}(I, \mathfrak{a}, t_{s+1})$ of infected neighbors. These numbers of infected neighbors are collected into the rate $\rho_{\mathfrak{N}}(D_i, t_{s+1})$ of infected neighbors:

$$\rho_{\mathfrak{N}}(D_i, t_{s+1}) = \frac{1}{N_i} \sum_{\mathfrak{a} \in \mathfrak{A}_i} \mathfrak{N}(I, \mathfrak{a}, t_{s+1}), \tag{12}$$

  where $\mathfrak{A}_i$ denotes the set of agents in region D_i, and N_i the number of agents in region i.
  - If the rate of infected neighbors overcomes a given threshold $\mathcal{T}_3$, that is $\rho_{\mathfrak{N}}(D_i, t_{s+1}) > \mathcal{T}_3$, then citizens decide to be in opposition with the protection strategy, which is determined by the mapping

$$u_i(t_{s+1}) = u_i(t_s) \times (1 + d_2),$$

    where d_2 is an opposition parameter such that $0 < d_2 < 1$. These opposition behaviors mean that policy makers loose the confidence of citizens, who are led to doubt on the protection strategy which is observed as inefficient.
  - Else, that is, if $\rho_{\mathfrak{N}}(D_i, t_{s+1}) \leq \mathcal{T}_3$, then citizens accept to decrease their level of opposition, which is determined by the mapping

$$u_i(t_{s+1}) = u_i(t_s) \times (1 - d_2).$$

The above protocol defines a discrete mapping

$$\lambda_{s+1} = G\big(X(t_{s+1}), \lambda_s\big), \tag{13}$$

which determines the microscopic part ($\mathfrak{m}_s$) of a hybrid model. Overall, with the system of ordinary differential equations (8) and the discrete mapping (13) derived from the above agent-based model, we have constructed a hybrid model of the form (AHP). In the sequel, our aim is to study the dynamics of the COVID-19 hybrid model (8)-(13). We already remark that the continuity assumption 1 on F is obviously satisfied; we shall demonstrate that assumption 2 is also always fulfilled, whereas assumption 3 is likely not to be satisfied.

Remark 4. The two actions protocol determined by (11) and (12) could easily be adapted to other decision strategies. For instance, if the rate $\rho_I(D_i, t_{s+1})$ of infected individuals in some region D_i $(1 \leq i \leq m)$ is less than the threshold $\mathcal{T}_1$, then it can be decided that the fraction of protected individuals is decreased, which would be modeled by setting

$$p_{i+1}(t_{s+1}) = p_i(t_s) \times (1 - d_1).$$

Similarly, a great number of decision strategies and behavioral changes can be integrated in the protocol, which shows the wide potential of application of our model.

Remark 5. We emphasize that the agent-based model determined by (11) and (12) is not an optimal strategy, since the decisions and their acceptance or opposition behaviors of the agents may produce a negative effect on the dynamic of the epidemic. However, the behavioral agent-based model allows us to introduce more reality on the analysis of epidemics dynamics than the just considering the deterministic compartmental model (8) and, for example, to study the impact of individuals behaviors on the spreading of an infection disease.

4. Analysis of the COVID-19 hybrid model.

In this section, we analyze the dynamics of the COVID-19 hybrid model (8)-(13). We prove that the model satisfies the compactness assumption 2, which guarantees that it admits global solutions. Then we study the local and global stability of its equilibrium states.

4.1. Uniformly invariant region and global solutions.

Let us consider the system of ordinary differential equations (8), where F is given by (9). We introduce the compact set $K \subset \mathbb{R}^{5m}$ defined by

$$K = \left\{ (S_i, A_i, I_i, R_i, P_i)_{1 \leq i \leq m} \in (\mathbb{R}^+)^{5m} \; ; \; \sum_{i=1}^{m} (S_i + A_i + I_i + R_i + P_i) \leq \frac{\Lambda_0}{\mu_0} \right\}, \tag{14}$$

where $\Lambda_0 = \sum_{i=1}^{m} \Lambda_i$ and $\mu_0 = \min\big\{\mu_i \; ; \; 1 \leq i \leq m\big\}$. The following theorem guarantees that the compact set K is an invariant region for the system of ordinary differential equations (8).

Theorem 4.1. *For any $X_0 \in K$ and any $\lambda_0 \in J$, the Cauchy problem given by (8) and $X(0) = X_0$ admits a unique solution denoted by $X(t, X_0, \lambda_0)$, defined on $[0, \infty)$, whose components are non-negative. Furthermore, the compact set K defined by (14) is positively invariant.*

Proof. First, the existence and uniqueness of local in time solutions is immediate, since F is polynomial. Next, the non-negativity of the components is guaranteed

by the quasi-positivity of the non-linear operator F, which means that it satisfies the property

$$F_j(x_1, \ldots, x_{j-1}, 0, x_{j+1}, \ldots, x_m, \lambda) \geq 0,$$

for all $(x_1, \ldots, x_m) \in (\mathbb{R}^+)^{5m}$, $j \in \{1, \ldots, m\}$ and $\lambda \in J$. By virtue of Proposition A.17 in [36], it follows that the components of any solution $X(t, X_0, \lambda_0)$ stemming from X_0 in K remain non-negative in future time.

Afterwards, it is easily seen that the total population in the geographical network, defined by

$$N(t) = \sum_{j=1}^{m} \big[S_j(t) + A_j(t) + I_j(t) + R_j(t) + P_j(t)\big], \quad t \geq 0,$$

satisfies

$$\dot{N}(t) \leq -\mu_0 N(t) + \Lambda_0, \quad t \geq 0,$$

since the matrix of connectivity L defined by (6) is a zero column sum matrix. By virtue of the Gronwall lemma, it follows that

$$N(t) \leq \left[N(0) - \frac{\Lambda_0}{\mu_0}\right] e^{-\mu_0 t} + \frac{\Lambda_0}{\mu_0}, \quad t \in [0, T],$$

which leads to the desired conclusion. □

The latter statement guarantees that the compactness assumption 2 is fulfilled. Hence, Theorem 2.2 applies to the COVID-19 hybrid model (8)-(13). We obtain the following corollary.

Corollary 1. *For any $(X_0, \lambda_0) \in K \times J$, the hybrid epidemiological model determined by (8) and (13) admits a unique global solution $X(t, X_0, \lambda_0)$ in the sense of definition 2.1.*

Remark 6. The latter corollary guarantees that the COVID-19 hybrid model (8)-(13) admits global solutions. However, the continuity assumption 3 on the function G given by (13) is very likely *not* to be satisfied. Indeed, even if the graph generation algorithm over the agents set (10) satisfies the continuity requirement (which would mean that two social networks are arbitrarily closed to each other, provided their corresponding agents sets are sufficiently closed), the decision protocol determined by (11) and (12) involves thresholds which can lead to discontinuities of the function G. In this case, the solutions of the COVID-19 hybrid model (8)-(13) can exhibit sensitive dynamics, as will be investigated in Section 5. This sensitivity of the system should not be seen as a pathology of the model, since it reproduces the complex dynamics of epidemics which can be very difficult to predict.

4.2. **Equilibrium points and basic reproduction number of the $SAIRP$ model with opposition behaviors.** Here we study the equilibrium states of the epidemiological model (3), which determines the local dynamics on each node of the complex network given by (7).

Basic computations show that the model (3) has two equilibrium points:

- disease-free equilibrium, denoted by Σ_0, given by

$$\Sigma_0 = (S_0, A_0, I_0, R_0, P_0) = \left(\frac{\Lambda\ (\omega + \mu)}{\mu\ (\phi p(1-u) + \mu + \omega)}, 0, 0, 0, \frac{\phi\, p\, (1-u)\, \Lambda}{\mu\ (\phi p(1-u) + \mu + \omega)}\right); \tag{15}$$

- endemic equilibrium, Σ_+, whenever $R_0 > 1$, given by

$$\Sigma_+ = (S_+, A_+, I_+, R_+, P_+) \tag{16}$$

with

$$\begin{aligned} S_+ &= \frac{\Lambda(\omega+\mu)}{(\phi p\,(1-u)+\mu+\omega)\mu} R_0^{-1}\,, \qquad A_+ = \frac{\Lambda}{\nu+\mu} R_0^{-1}(R_0-1)\,, \\ I_+ &= \frac{\Lambda\nu}{(\nu+\mu)(\delta+\mu)} R_0^{-1}(R_0-1)\,, \\ R_+ &= \frac{\delta\Lambda\nu}{(\nu+\mu)(\delta+\mu)\mu} R_0^{-1}(R_0-1)\,, \quad P_+ = \frac{\Lambda\phi p\,(1-u)}{(\phi p\,(1-u)+\mu+\omega)\mu} R_0^{-1}\,, \end{aligned} \tag{17}$$

where the basic reproduction number, R_0, is given by

$$R_0 = \frac{\beta\ (1-p\,(1-u))\,(\delta\,\theta+\mu\,\theta+\nu)\,(\omega+\mu)}{(\delta+\mu)\,(\nu+\mu)\,(\phi p\,(1-u)+\mu+\omega)}\,. \tag{18}$$

In what follows, we analyse the influence of the parameters p and u on the values of R_0. The partial derivatives of R_0 with respect to p and u are given by, respectively,

$$\begin{aligned} \frac{\partial R_0}{\partial p} &= -\frac{(\delta\,\theta+\mu\,\theta+\nu)\,(\mu+\omega)\,\beta\ (1-u)\,(\mu+\omega+\phi)}{(\delta+\mu)\,(\mu+\nu)\,(p\phi(1-u)+\mu+\omega)^2}\,, \\ \frac{\partial R_0}{\partial u} &= \frac{(\delta\,\theta+\mu\,\theta+\nu)\,(\mu+\omega)\,\beta\,p\,(\mu+\omega+\phi)}{(\delta+\mu)\,(\mu+\nu)\,(p\phi(1-u)+\mu+\omega)^2}\,. \end{aligned}$$

As all parameter values assume positive values and $0 < p, u < 1$ we have $\frac{\partial R_0}{\partial u} > 0$ and $\frac{\partial R_0}{\partial p} < 0$. Meaning that R_0 increases with u, but decreases as p increases.

In order to observe this variation of R_0 for different values of p and u, let us assume, fixed values for the parameters (see Tables 1-2):

$$\mu = \frac{1}{81\times 365},\ \theta = 1,\ \phi = \frac{1}{12},\ \nu = 0.15,\ \delta = \frac{1}{30},\ \omega = \frac{1}{45}\times 0.059,\ \beta = 1.492. \tag{Pfixed}$$

Then,

$$R_0(p,u) \simeq 0.0734993\,\frac{1-p(1-u)}{\frac{1}{12}p(1-u)+0.0013449}\,.$$

Let $0.25 \le p \le 0.675$ and $0 \le u \le 0.4$, then there holds $0.4147461 \le R_0(p,u) \le 4.5124381$, see Figure 3.

4.3. **Stability analysis of the equilibrium points.** The Jacobian matrix of system (3), evaluated at the disease-free equilibrium (15), is given by

$$M\,(\Sigma_0) = \begin{bmatrix} -(\phi\,p\,(1-u)+\mu) & \Theta_1 & -\frac{\beta\,(\mu+\omega)(1-p(1-u))}{\phi\,p(1-u)+\mu+\omega} & 0 & \omega \\ 0 & \Theta_2 & \frac{\beta\,(\mu+\omega)(1-p(1-u))}{\phi\,p(1-u)+\mu+\omega} & 0 & 0 \\ 0 & \nu & -\delta-\mu & 0 & 0 \\ 0 & 0 & \delta & -\mu & 0 \\ \phi\,p(1-u) & 0 & 0 & 0 & -(\mu+\omega) \end{bmatrix},$$

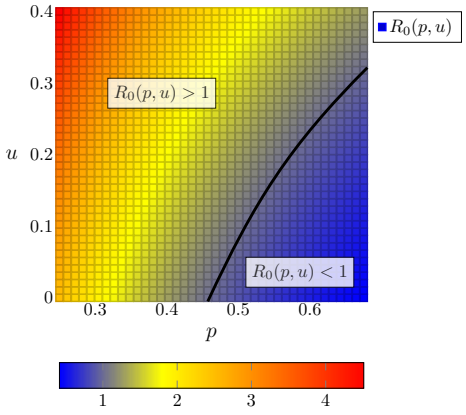

FIGURE 3. Basic reproduction number $R_0(p,u)$ of the $SAIRP$ model (3), with $0.25 \leq p \leq 0.675$ and $0 \leq u \leq 0.4$.

with

$$\Theta_1 = -\frac{\theta\,\beta\,(\mu+\omega)\,(1-p(1-u))}{\phi\,p(1-u)+\mu+\omega},$$
$$\Theta_2 = \frac{\beta\theta(1-p(1-u))(\mu+\omega)-(\mu+\nu)(p(1-u)\phi+\mu+\omega)}{\phi\,p(1-u)+\mu+\omega}.$$

The eigenvalues of the matrix $M(\Sigma_0)$ are given by $\lambda_1 = \lambda_2 = -\mu$, $\lambda_3 = -(\phi p(1-u)+\mu+\omega)$ and the remaining two, λ_4 and λ_5, are the roots of the polynomial $P(\lambda)$ given by

$$P(\lambda) = \lambda^2 + B\lambda + C,$$

where $B = \frac{-\beta\theta(1-p(1-u))(\omega+\mu)}{(p(1-u)\phi+\mu+\omega)}+\delta+2\mu+\nu$ and $C = \frac{\mathcal{D}-\mathcal{N}}{p(1-u)\phi+\mu+\omega}$. The local stability of the disease-free equilibrium Σ_0 comes by the application of the Routh–Hurwitz criterion, if, and only if, $B > 0$ and $C > 0$. It is easy to show that $C > 0$ whenever $R_0 < 1$. The proof that $B > 0$ is positive whenever R_0 is analogous to the one made in [34] replacing p by $p(1-u)$. We have just proved the following theorem.

Theorem 4.2. *The disease free equilibrium of the $SAIRP$ model (3), Σ_0 given by (15), is locally asymptotically stable whenever $R_0 < 1$.*

To analyze the local stability of the endemic equilibrium, Σ_+, we evaluate the Jacobian matrix of system (3) at the endemic equilibrium (17), here denoted by $M(\Sigma_+)$ (we do not write the expression of $M(\Sigma_+)$ due to the long size of each terms). We follow by computing the characteristic equation, given by,

$$Q(t) = \left|\lambda I_5 - M(\Sigma_+)\right| = 0\,,$$

where I_5 represents the identity matrix of dimension 5.

The roots of the equation $Q(t) = 0$ are however hard to analyze analytically. Therefore, here we study the local stability of Σ_+ considering fixed parameter values (Pfixed). For these parameter values, the characteristic equation $Q(t) = 0$ is given by

$$0.0012388\,(\lambda + 0.0000338)\left(807.1694484\,\lambda^4 + A_3\lambda^3 + A_2\lambda^2 + A_1\lambda + A_0\right) = 0\,, \tag{19}$$

with

$$\begin{aligned}
A_3 &\simeq \beta\,(1-p\,(1-u)) + 65.5724947\,p\,(1-u) + 127.0843058\\
A_2 &\simeq 0.1847459\,\beta\,(1-p\,(1-u)) + 10.1896471\,p\,(1-u) + 0.1687146\,,\\
A_1 &\simeq 0.0052528\,\beta\,(1-p\,(1-u)) - 0.0085307\,p\,(1-u) - 0.0001376\\
A_0 &\simeq 0.0000067\,\beta\,(1-p\,(1-u)) - 0.0000113\,p\,(1-u) - 0.0000002\,.
\end{aligned}$$

Applying the Routh–Hurwitz criterion to the fourth order polynomial (19), the endemic equilibrium Σ_+ is locally asymptotically stable whenever the following inequalities hold:

$$A_0 > 0\,,\quad A_3 > 0\,,\quad A_3A_2 - A_4A_1 > 0\,,\quad C = (A_3A_2 - A_4A_1)\,A_1 - A_3^2A_0 > 0\,. \tag{20}$$

The conditions $A_0 > 0$ and $A_3 > 0$ hold for all positive $0 < p, u \leq 1$. As for the conditions $A_3A_2 - A_4A_1 > 0$ and $C > 0$, we assume the parameter values (Pfixed) and observe that they hold whenever $R_0(u,p) > 1$, for $0.25 \leq p \leq 0.675$ and $0 \leq u \leq 0.4$, see Figure 4.

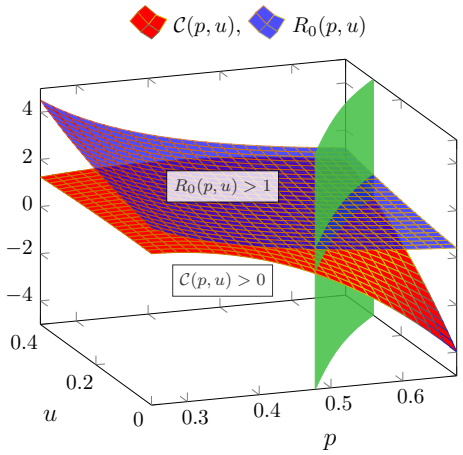

FIGURE 4. Local stability condition of the endemic equilibrium Σ_+ is satisfied for $R_0(p,u) > 1$. Considering the parameter values (Pfixed) and varying $0.25 \leq p \leq 0.675$, $0 \leq u \leq 0.4$.

Remark 7. Note that the global stability of the disease free and endemic equilibrium points Σ_0 and Σ_+ can also be established; the proofs are analogous to the ones made in [34], replacing p by $p(1-u)$.

4.4. **Fit the *SAIRP* model with COVID-19 data in Portugal.** The *SAIRP* model with piecewise constant parameters presented in [34], can be used to fit the real data of active infected individuals with COVID-19, for a fixed period of time and for a single region. Here we consider the number of active infected individuals with COVID-19 in Portugal from the date of the first confirmed case, March 2, 2020, until April 15, 2021 (the data can be found in [11]). We consider a time interval of 410 days which we subdivide into 9 sub-intervals based on the behavior of the epidemic curve and the public health policies imposed by the Portuguese Government. For

each sub-interval of time, the parameters β, f and p take piecewise constant values and we assume $u = 0$. See Table 1 for the time sub-intervals and the corresponding piecewise constants parameter values. The remaining parameter values are fixed and take the values presented in Table 2.

However, the piecewise constant parameters model does not integrate at the microscopic scale the impact of opposition behaviors to policy strategies; moreover, it does not take into account the geographical distribution of individuals. Thus our aim in the next section is to deeper explore the dynamics of the hybrid model (8)-(13), with a numerical approach.

TABLE 1. Piecewise parameter values β_i, p_i, m_i, for $i = 1, \ldots, 9$, of the $SAIRP$ model.

Time sub-interval	β_i (transmission rate)	p_i (transfer from S to P)	f_i (transfer from P to S)
$[0, 73]$	$\beta_1 = 1.502$	$p_1 = 0.675$	$f_1 = 0.066$
$[73, 90]$	$\beta_2 = 0.600$	$p_2 = 0.650$	$f_2 = 0.090$
$[90, 130]$	$\beta_3 = 1.240$	$p_3 = 0.580$	$f_3 = 0.180$
$[130, 163]$	$\beta_4 = 0.936$	$p_4 = 0.610$	$f_4 = 0.160$
$[163, 200]$	$\beta_5 = 1.531$	$p_5 = 0.580$	$f_5 = 0.170$
$[200, 253]$	$\beta_6 = 0.886$	$p_6 = 0.290$	$f_6 = 0.140$
$[253, 304]$	$\beta_7 = 0.250$	$p_7 = 0.370$	$f_7 = 0.379$
$[304, 329]$	$\beta_8 = 0.793$	$p_8 = 0.370$	$f_8 = 0.090$
$[329, 410]$	$\beta_9 = 0.100$	$p_9 = 0.550$	$f_9 = 0.090$

TABLE 2. Constant parameter values and initial conditions for $SAIRP$ model, see [34].

Parameter	Description	Value
Λ	Recruitment rate	$\frac{0.19\% \times N_0}{365}$
μ	Natural death rate	$\frac{1}{81 \times 365}$
θ	Modification parameter	1
v	Transfer rate from A to I	1
q	Fraction of A individuals confirmed as infected	0.15
ϕ	Transfer rate from S to P	$\frac{1}{12}$
δ	Transfer rate from I to R	$\frac{1}{27}$
w	Transfer rate from P to S	$\frac{1}{45}$
Class of individuals	Initial condition value	
Susceptible	$S(0) = 10295894$	
Asymptomatic	$A(0) = \frac{2}{0.15}$	
Active infected	$I(0) = 2$	
Removed	$R(0) = 0$	
Protected	$P(0) = 0$	

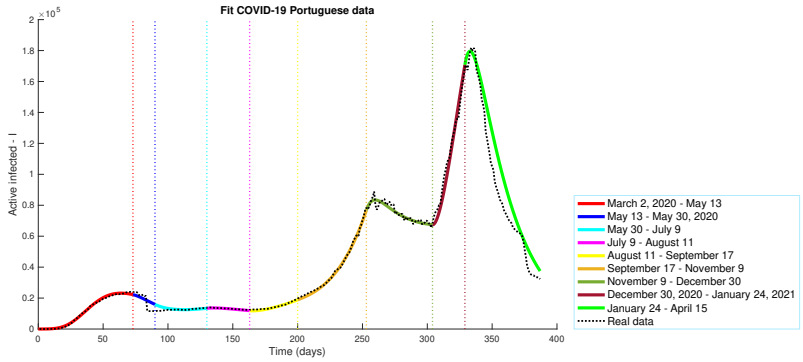

FIGURE 5. Model $SAIRP$ with parameter values from Tables 1-2 (colored continuous line) fitting the real data (discontinuous line) of active infected individuals with COVID-19 in Portugal, from March 2, 2020 until April 15, 2021.

5. **Numerical simulations of the COVID-19 hybrid model.** In this section, our aim is to explore numerically the dynamics of the hybrid model (8)-(13), in order to show how and to what extent individual behaviors can influence the dynamic of the epidemic. The hybrid problem has been implemented with the `python` language, using the library `networkx`, which integrates graph generation algorithms. We consider an abstract geographical network of 5 regions (depicted in Figure 6), which is inspired from the complex network studied in [34]; the connectivity matrix of this geographical network is given by

$$L = \begin{bmatrix} -\varepsilon_{21} & \varepsilon_{12} & 0 & 0 & 0 \\ \varepsilon_{21} & -(\varepsilon_{12}+\varepsilon_{32}+\varepsilon_{42}) & \varepsilon_{23} & \varepsilon_{24} & 0 \\ 0 & \varepsilon_{32} & -(\varepsilon_{23}+\varepsilon_{43}) & \varepsilon_{34} & 0 \\ 0 & \varepsilon_{42} & \varepsilon_{43} & -(\varepsilon_{24}+\varepsilon_{34}+\varepsilon_{54}) & \varepsilon_{45} \\ 0 & 0 & 0 & \varepsilon_{54} & -\varepsilon_{45} \end{bmatrix},$$

where we assume a weak and homogeneous connectivity by setting $\varepsilon_{ij} = 0.1$ for all $i, j \in \{1, \ldots, 5\}$. The coupling strengths are given by $\sigma_S = \sigma_A = 0.1$ and $\sigma_I = \sigma_R = \sigma_P = 0$, which means that only susceptible and asymptomatic individuals present a spatial mobility. The values of other parameters are given in Table 3. We have chosen these parameter values so that the endemic equilibrium is stable in the regions 1, 2, 3, whereas the disease free equilibrium is stable in the two other regions. In other words, in absence of couplings in the geographical network, the orbits of the model (3) are attracted to Σ^+ in three regions, whereas they are attracted to Σ_0 in two other regions. Each social network is generated by running a Watts-Strogatz small-world algorithm in which each agent has 10 neighbors at most, and where the probability of rewiring each edge is fixed to 0.02. In this way, we generate a set of agents $\mathfrak{A}_{ij}$, as detailed in Subsection 3.3, whose structure reproduces the main social interactions in a group of individuals (see [31]). Now we investigate the effects of individual behaviors on the dynamics of the hybrid model, by testing four relevant scenarios, which are presented and discussed below. To this end, we solve the hybrid model (8)-(13) on a fixed timeline and store the outputs of the agent-based process

(11)-(12) in data files. The results of the numerical simulations are illustrated in Figure 7: each sub-figure shows the number of infected individuals $I_i(t)$ of one region D_i $(1 \leq i \leq 5)$, for the four selected scenarios, and a comparison with the simulation of the "only-macroscopic" model (8). In these four scenarios, we fix the end of the timeline (1) at $T = 50$ and we focus on a variation of the number N of steps along this timeline, the thresholds $\mathcal{T}_1$, $\mathcal{T}_2$, $\mathcal{T}_3$ and the decision parameters d_1, d_2 involved in the agent-based model given by (11) and (12). Obviously, all parameter values could be modified for testing other relevant scenarios. For instance, the influence of the topology of the geographical network has been discussed (for a non-hybrid model) in [7].

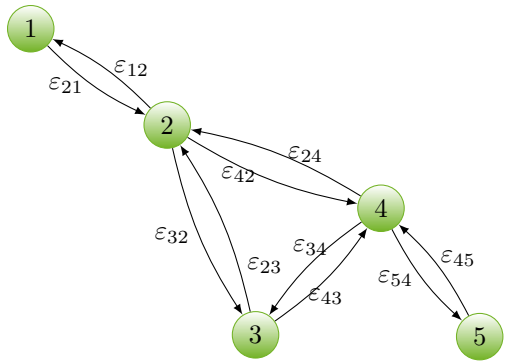

FIGURE 6. A geographical network with 5 regions and the main connections. Individual displacements from one region to another occur along these connections.

5.1. **Scenario 1: infection under control with fast confinement decision.** In the first scenario, we divide the timeline (1) of the hybrid model in $N = 60$ sub-intervals of constant width. The decision parameters and the thresholds involved in the agent-based protocol (11)-(12) are given by

$$d_1 = 0.1, \quad \mathcal{T}_1 = 0.02, \quad \mathcal{T}_2 = 0.03, \quad d_2 = 0.01, \quad \mathcal{T}_3 = 0.3.$$

These numerical values have been chosen arbitrarily and could easily be modified. With those parameter values, we observe, as depicted in green in Figure 7, that the numbers of infected individuals $I_i(t)$ decrease to 0 in each region D_i $(1 \leq i \leq 5)$. More specifically, the output of the agent-based process leads to a first decision of confinement (induced by Action 1 in the protocol (11)-(12)) from $t = 0$ until $t = 0.8$ and a second decision of confinement from $t = 4.9$ until $t = 8.2$. These decisions of confinement are favored by a low value of the threshold $\mathcal{T}_2$. In parallel, the weak value of the parameter d_2 means minority opposition behaviors in the population. By comparison with the output of the only-macroscopic model given by the system (8) (which is depicted in red in Figure 7), we observe that the decision protocol with fast confinement decision, succeeds in avoiding the persistence of the disease in the whole population. We also note a particular situation in region 5: the hybrid model does not modify the decrease of infection to 0, which is guaranteed by a low basic reproduction number ($R_0 \simeq 0.0375$, see Table 3) and also the geographical position

TABLE 3. Values of the parameters for the numerical simulations of the hybrid model (8).

Parameter	**Region 1**	**Region 2**	**Region 3**	**Region 4**	**Region 5**
β	2	2	2	0.1	0.1
p	0.0	0.0	0.0	0.5	0.5
θ	1	1	1	1	1
Λ	1000	1000	1000	1	1
ϕ	1	1	1	1	1
ω	1	1	1	1	1
μ	1	1	1	1	1
ν	1	1	1	1	1
δ	1	1	1	1	1
u	0.2	0.2	0.2	0.2	0.2
R_0	1.3269	1.3269	1.3269	0.0375	0.0375
Initial condition	**Region 1**	**Region 2**	**Region 3**	**Region 4**	**Region 5**
S_0	297.24	140.39	358.32	151.39	443.33
A_0	13.33	6.66	6.66	13.33	6.66
I_0	2	1	1	2	1
R_0	0	0	0	0	0
P_0	0	0	0	0	0

of region 5, which is not connected to regions 1, 2, 3, where the basic reproduction number is greater than 1.

5.2. **Scenario 2: postponed extinction of the disease by slowness in the decision process.** In the second scenario, we divide the timeline (1) in $N = 20$ sub-intervals of constant width. In this way, the first execution of the agent-based process (11)-(12) occurs at $t = 2.5$, whereas it occurs at $t \simeq 0.83$ in the first scenario. This choice roughly models a slowness decision process. Other parameters are still given by

$$d_1 = 0.1, \quad \mathcal{T}_1 = 0.02, \quad \mathcal{T}_2 = 0.03, \quad d_2 = 0.01, \quad \mathcal{T}_3 = 0.3.$$

As depicted in blue in Figure 7, we observe that the numbers of infected individuals $I_i(t)$ still decrease to 0 in each region D_i $(1 \leq i \leq 5)$. However, the decrease is postponed with respect to scenario 1. Indeed, the output of the agent-based model (11)-(12) leads to a single decision of confinement, from $t = 4.8$ until $t = 14.3$. Overall, the decision of confinement is made later and its duration is longer than in scenario 1, which leads to a postponed extinction of the disease. It is also interesting to observe the emergence of small waves in region 4; these small waves seem to be caused by the connections with regions 1, 2, 3, where the decrease of infection is postponed.

5.3. **Scenario 3: postponed extinction of the disease by opposition behaviors.** In the third scenario, our aim is to explore the possible conflict between a slow decision process of policy makers (as described by Action 1 in the agent-based protocol (11)-(12)) and a high level of opposition behaviors of citizens (determined by Action 2 in the protocol (11)-(12)). To that aim, we still divide the timeline (1)

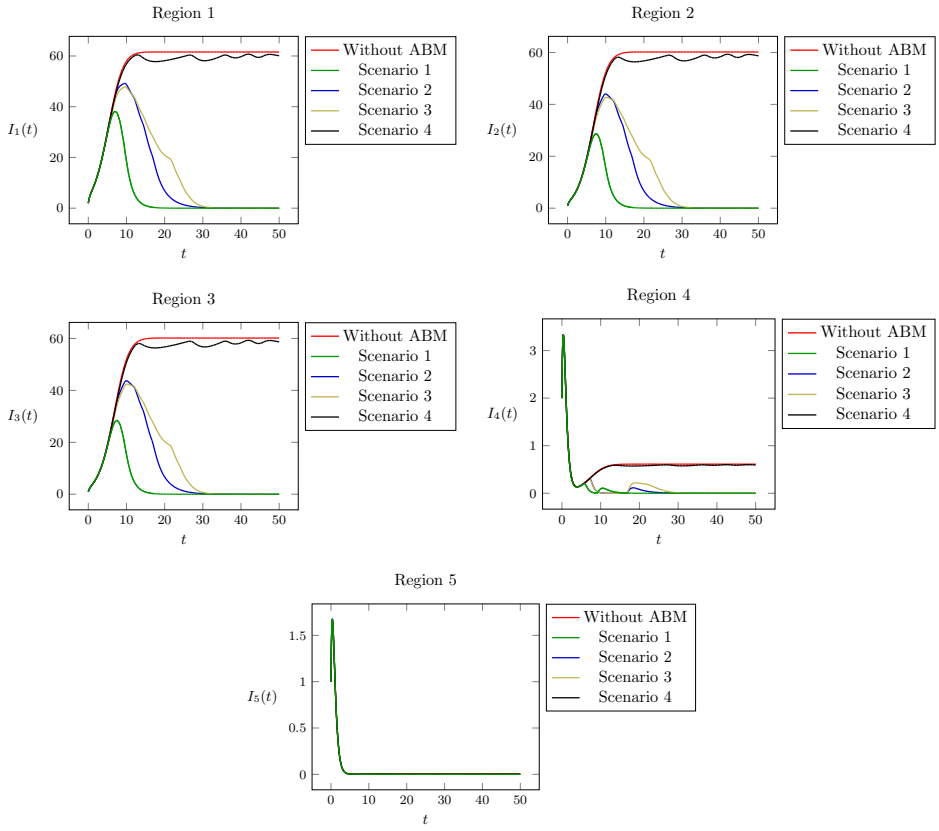

FIGURE 7. Numerical simulations of the hybrid model (8)-(13), for four relevant scenarios. Each sub-figure shows the number $I_i(t)$ of infected individuals in each region D_i $(1 \leq i \leq 5)$ of the geographical network depicted in Figure 6.

in $N = 20$ sub-intervals of constant width; the values of d_1, $\mathcal{T}_1$ and $\mathcal{T}_2$ are the same as in scenarios 1 and 2, whereas we modify the values of the opposition behaviors parameters by setting

$$d_2 = 0.09, \quad \mathcal{T}_3 = 0.2.$$

This choice roughly models an increase of opposition behaviors in the population and a lower threshold of acceptation of protection strategies. As depicted in dark yellow in Figure 7, we observe that the infection is still under control, but the extinction of the disease is almost postponed by the opposition behaviors. Moreover, we remark that the small infection waves, which were already observed in region 4 with scenario 2, are amplified.

5.4. **Scenario 4: emergence of multiple pandemic waves due to risk negation.** In the fourth scenario, we divide the timeline (1) in $N = 60$ sub-intervals of constant width. We come back to minority opposition behaviors as in scenarios 1 and 2 by setting $d_2 = 0.01$, $\mathcal{T}_3 = 0.3$, but we modify the decision of confinement

parameters by assuming

$$d_1 = 0.1, \quad \mathcal{T}_1 = 0.06, \quad \mathcal{T}_2 = 10^3.$$

The value of the threshold $\mathcal{T}_1$ is greater than in other scenarios, which means that the decision of protection are postponed; in parallel, the value of the threshold $\mathcal{T}_2$ is much greater, which means that the control strategy does not consider seriously confinement as a major decision, or even that confinement should be avoided, for example in order to maintain the economic activity, at the risk to exacerbate the level of infection. In this case, we observe, as depicted in black in Figure 7, that the level of infection does not decrease to 0, except in region 5, which is not connected to the regions where the basic reproduction number is greater than 1. We observe the emergence of infection oscillations around a level which corresponds to the persistence of the disease in the non-hybrid model (8). The emergence of such oscillations was predicted by Theorem 2.4. It suggests that the negation of the health risk by decision makers could compromise the control of the epidemic. We also indicate that a small perturbation of the parameters d_1 and $\mathcal{T}_1$ can amplify or destroy these oscillations, which might correspond to a bifurcation process in the hybrid model (8)-(13).

6. **Conclusion and future work.** In this paper, we have brought an original contribution to the study of complex systems arising in social science, economics and epidemiology, by constructing a class of hybrid models, in which the macroscopic dynamics of a population subject to an evolution problem, were coupled with the microscopic dynamics of individuals. The macroscopic dynamics was modeled by a system of differential equations, embedded in a geographical network structure, whereas the microscopic dynamic was modeled by an agent-based process, which can integrate various individual behaviors. The transition between the macroscopic and the microscopic scales involves the generation of a social network, which reproduces the social interactions occurring in the population. Our hybrid model was studied in an abstract and theoretical framework, by establishing the existence and uniqueness of relevant solutions, their continuous dependence with respect to a variation of its parameters and the possible emergence of pseudo-periodic solutions. We applied our hybrid model to the study of the current COVID-19 pandemic, and performed several numerical simulations, which highlight how microscopic behaviors can have a strong impact on the macroscopic of the epidemic.

As future work, we aim to generalize our hybrid framework, by considering a larger class of dynamical systems modeling the macroscopic dynamic of the population: for example, non-autonomous equations, delay differential equations or reaction-diffusion equations could be considered. Analogously, the agent-based process studied in Section 3, can be subject to various generalizations, which show the wide potential of the hybrid approach. Moreover, it is also a challenge to improve the SAIRP model by considering specific subgroups for the protected class P distinguishing the different protective measures that may be applied to control the epidemic. We also aim to investigate a question which was left open in the present paper: the emergence of unstable oscillations under an increase of opposition behaviors has been observed, and will be deeper investigated in a separate work.

Acknowledgments. This work was partially supported by Portuguese funds through CIDMA, The Center for Research and Development in Mathematics and Applications of University of Aveiro, and the Portuguese Foundation for Science and Technology (FCT–Fundação para a Ciência e a Tecnologia), within project UIDB/04106/2020. Silva is also supported by the FCT Researcher Program CEEC Individual 2018 with reference CEECIND/00564/2018.

The authors are sincerely grateful to the anonymous reviewers for their valuable comments and suggestions which improved the presentation of the paper.

REFERENCES

[1] M. Ajelli, B. Gonçalves, D. Balcan, V. Colizza, H. Hu, J. J. Ramasco, S. Merler and A. Vespignani, Comparing wide-scale computational modeling Approaches to epidemic: Agent-based versus structured MetaPopulation models, *BMC Infectious Diseases*, **10** (2010), Article number: 190.

[2] L. J. S. Allen, *An Introduction to Stochastic Processes with Applications to Biology*, Second edition. CRC Press, Boca Raton, FL, 2011.

[3] L. J. S. Allen and E. J. Allen, A comparison of three different stochastic population models with regard to persistence time, *Theoretical Population Biology*, **64** (2003), 439–449.

[4] A. Banos, N. Corson, B. Gaudou, V. Laperrière and S. R. Coyrehourcq, The importance of being hybrid for spatial epidemic models: a multi-scale approach, *Systems*, **3** (2015), 309–329.

[5] A. Banos, C. Lang and M. Nicolas, *Agent-based Spatial Simulation with NetLogo*, Elsevier, 2017.

[6] G. Cantin, Nonidentical coupled networks with a geographical model for human behaviors during catastrophic events, *International Journal of Bifurcation and Chaos*, **27** (2017), 1750213, 21pp.

[7] G. Cantin and C. J. Silva, Influence of the topology on the dynamics of a complex network of HIV/AIDS epidemic models, *AIMS Mathematics*, **4** (2019), 1145–1169.

[8] Centers for Disease Control and Prevention, *Coronavirus Disease 2019 (COVID-19)*, 2020. Available from: https://www.cdc.gov/coronavirus/2019-ncov/prevent-getting-sick/prevention.html.

[9] V. Colizza and A. Vespignani, Epidemic modeling in metapopulation systems with heterogeneous coupling pattern: Theory and simulations, *Journal of theoretical biology*, **251** (2008), 450–467.

[10] E. Delisle, C. Rousseau, B. Broche, I. Leparc-Goffart and others, Chikungunya outbreak in Montpellier, France, September to October 2014, *Eurosurveillance*, **20** (2015), 21108.

[11] Direção Geral da Saúde – COVID-19 *Ponto de Situação Atual em Portugal*, 2021. Available from: https://covid19.min-saude.pt/ponto-de-situacao-atual-em-portugal/.

[12] M. Dolfinand M. Lachowicz, Modeling opinion dynamics: how the network enhances consensus, *Networks & Heterogeneous Media*, **10** (2015), 877–896.

[13] A. Ducrot and P. Magal, Travelling wave solutions for an infection-age structured model with diffusion, *Proc. Roy. Soc. Edinburgh Sect. A*, **139** (2009), 459–482.

[14] J. M. Epstein, J. Parker, D. Cummings and R. A. Hammond, Coupled contagion dynamics of fear and disease: Mathematical and computational explorations, *PLoS One*, **3** (2008), e3955.

[15] European Centre for Disease Prevention and Control, *Guidelines for the Implementation of Non-Pharmaceutical Interventions Against COVID-19*, 2020. Available from: https://www.ecdc.europa.eu/en/publications-data/covid-19-guidelines-non-pharmaceutical-interventions.

[16] L. Fahse, C. Wissel and V. Grimm, Reconciling classical and individual-based approaches in theoretical population ecology: A protocol for extracting population parameters from individual-based models, *The American Naturalist*, **152** (1998), 832–856.

[17] S. Galam, *Sociophysics: A Physicist's Modeling of Psycho-political Phenomena*, Understanding Complex Systems. Springer, New York, 2012.

[18] S. Grauwin, E. Bertin, R. Lemoy and P. Jensen, Competition between collective and individual dynamics, *Proceedings of the National Academy of Sciences*, **106** (2009), 20622–20626.

[19] J. K. Hale, *Ordinary Differential Equations*, Krieger Publishing Company (second edition), 1980.

[20] D. Helbing, *Quantitative Sociodynamics: Stochastic Methods and Models of Social Interaction Processes*, Springer-Verlag Berlin Heidelberg, 2010.
[21] A. J. Heppenstall, A. T. Crooks, L. M. See and M. Batty, *Agent-based Models of Geographical Systems*, Springer Science & Business Media, 2011.
[22] H. W. Hethcote, Three basic epidemiological models, in *Applied Mathematical Ecology*, Springer, **18** (1989), 119–144.
[23] H. W. Hethcote and P. Van den Driessche, Some epidemiological models with nonlinear incidence, *Journal of Mathematical Biology*, **29** (1991), 271–287.
[24] D. A. Jones, H. L. Smith and H. R. Thieme, Spread of viral infection of immobilized bacteria, *Networks & Heterogeneous Media*, **8** (2013), 327–342.
[25] W. O. Kermack and A. G. McKendrick, Contributions to the mathematical theory of epidemics–I. 1927, *Bulletin of mathematical biology*, **53** (1991), 33–55.
[26] K. Klemm, M. Serrano, V. M. Eguíluz and M. San Miguel, A measure of individual role in collective dynamics, *Scientific Reports*, **2** (2012), Article number: 292, 8pp.
[27] E. Logak and I. Passat, An epidemic model with nonlocal diffusion on networks, *Networks & Heterogeneous Media*, **11** (2016), 693–719.
[28] N. Marilleau, C. Lang and P. Giraudoux, Coupling agent-based with equation-based models to study spatially explicit megapopulation dynamics, *Ecological Modelling*, **384** (2018), 34–42.
[29] C. McPhail and R. T. Wohlstein, Individual and collective behaviors within gatherings, demonstrations, and riots, *Annual Review of Sociology*, **9** (1983), 579–600.
[30] J. D. Murray, *Mathematical Biology II: Spatial Models and Biomedical Applications*, Third edition. Interdisciplinary Applied Mathematics, 18. Springer-Verlag, New York, 2003.
[31] M. E. J. Newman and D. J. Watts, Scaling and percolation in the small-world network model, *Physical Review E*, **60** (1999), 7332.
[32] N. D. Nguyen, *Coupling Equation-based and Individual-based Models in the Study of Complex Systems. A Case Study in Theoretical Population Ecology*, Ph.D thesis, Pierre and Marie Curie University, 2010.
[33] F. Schweitzer, *Self-organization of Complex Structures: From Individual to Collective Dynamics*, Gordon and Breach Science Publishers, Amsterdam, 1997.
[34] C. J. Silva, G. Cantin, C. Cruz, R. Fonseca-Pinto, R. P. Fonseca, E. S. Santos and D. F. M. Torres, Complex network model for COVID-19: human behavior, pseudo-periodic solutions and multiple epidemic waves, *Journal of Mathematical Analysis and Applications*, (2021), 125171.
[35] C. J. Silva, C. Cruz, D. F. M. Torres et al., Optimal control of the COVID-19 pandemic: Controlled sanitary deconfinement in Portugal, *Scientific Reports*, **11** (2021), Art. 3451, 15 pp.
[36] H. L. Smith and H. R. Thieme, *Dynamical Systems and Population Persistence*, American Mathematical Soc., Providence, RI, 2011.
[37] R. H. Turner, L. M. Killian and others, *Collective Behavior*, Prentice-Hall Englewood Cliffs, NJ, 1957.
[38] S. Wright, *Crowds and Riots: A Study in Social Organization*, Sage Publications Beverly Hills, CA, 1978.
[39] P. Yan and G. Chowell, Beyond the initial phase: Compartment models for disease transmission, in *Quantitative Methods for Investigating Infectious Disease Outbreaks* (Texts in Applied Mathematics), Springer, Cham, **70** (2019), 135–182.

Received May 2021; revised November 2021; early access March 2022.

E-mail address: guillaume.cantin@univ-nantes.fr
E-mail address: cjoaosilva@ua.pt
E-mail address: arnaud.banos@cnrs.fr